Vibrational Coherence Transfer and Trapping as Sources for Long-Lived Quantum Beats in Polarized Emission from Energy Transfer Complexes

Jeffrey A. Cina*,†,‡ and Graham R. Fleming*,‡

Department of Chemistry and Oregon Center for Optics, University of Oregon, Eugene, Oregon 97403, and Department of Chemistry, University of California, Berkeley and Physical Biosciences Division, Lawrence Berkeley National Laboratory, Berkeley, California 94720

Received: July 6, 2004; In Final Form: September 23, 2004

We entertain vibrational coherence transfer and related processes as possible sources for certain long-lived quantum beats observed in time-resolved polarized emission signals from photosynthetic light harvesting complexes. Signal calculations on a dimer model in which each chromophore supports a single vibrational mode show that coherence transfer to the acceptor and coherence trapping in the donor can increase the longevity of vibronic quantum beats beyond the time-scale for electronic energy exchange. These mechanisms imply an active role for coherent vibrational motion in the time-course of ultrafast energy transfer and suggest that external control over vibrations may provide a means for influencing the transport of electronic excitations. The effects of vibrational coherence transfer and trapping on excitation transfer are most vivid when the excitation−vibration coupling strength exceeds that for energy transfer. In light of the strong transfer coupling of photosynthetic light-harvesting complexes, we also examine the adiabatic energy-transfer regime, in which the relative coupling strengths are reversed.

I. Introduction

In the ultrafast spectroscopic study of photosynthetic light-harvesting complexes, oscillatory components of the signals are frequently observed.[1−6] For example, the time-resolved polarized emission data from bacteriochlorophyll in the core light-harvesting antenna (LH1) of photosynthetic bacteria exhibit 105 cm^{-1} oscillations suggestive of wave packet motion in the excited electronic state.[1] As this wavenumber lies in the range of low-frequency modes observed in the reaction center special pair,[7,8] these quantum beats were taken as supporting evidence for some degree of bacteriochlorophyll dimerization in LH1, whose crystal structure has only recently been elucidated at 4.8 Å.[9] Interestingly, the damping of those oscillations takes longer than the depolarization time-scale as determined from the decay of the emission anisotropy.

The long-lived nature of these putatively vibrational quantum beats in LH1 has remained puzzling, as it seems to conflict with an expected degradation of vibrational coherence during the electronic energy transfer process.[1,10] Because they exhibit prominent long-lived vibrational oscillations, the data of Bradforth et al.[1] and related results[2−6] give evidence for a measure of involvement by optically active nuclear modes in photosynthetic electronic energy transfer. Quantum beats in the polarized emission lasting longer than the characteristic energy transfer time are difficult to reconcile with an incoherent (Förster) model of short-time photosynthetic energy transfer. That widely applicable theory[11−13] has been successfully applied to many systems over times long enough that the molecular and lattice vibrations can be assumed to have relaxed fully prior to energy transfer.

The purpose of this article is to investigate the influence of coherent molecular vibrations on the short-time dynamics of electronic excitation transfer as observed in polarized time-resolved emission and to clarify their effects in various regimes of excitation-vibration and excitation-transfer coupling strength. We explore the time-resolved emission from a model energy-transfer complex consisting of a pair of chromophores of fixed relative orientation and coupling strength. Each chromophore supports a single Franck−Condon active vibrational mode. To investigate the effects on energy transfer of the vibronic superposition states launched by short-pulse excitation−and vice versa−we omit vibrational relaxation and dephasing, except for that induced by excitation transfer between the chromophores and by independent static inhomogeneities in the electronic site energies of the two chromophores.

We present rigorously calculated emission signals for this model system with physically reasonable parameter values for the energy-transfer coupling strength, the displacement of the Franck−Condon active vibrational modes, and the ultrashort pulse durations. In keeping with our specific interest in the coupled dynamics of vibrations and electronic excitation transfer between identical bacteriochlorophyll molecules in light-harvesting complexes, we focus primarily on the case of equal site energies, but also investigate the behavior of coherent vibrations in downhill energy transfer. For the limiting case of strong excitation-transfer coupling and weak excitation-vibration coupling, we present physically illuminating analytic expressions for the polarized emission and compare them to numerical calculations.

In the case of equal site energies, our calculated time-resolved polarized emission signals and the emission anisotropy exhibit behavior strikingly reminiscent of that seen in LH1.[14] We see sustained vibrational quantum beats that are in phase between parallel and perpendicular emission. Although there is some indication of critically- or slightly overdamped coherent cycling

* To whom correspondence should be addressed. E-mail: cina@uoregon.edu (J.A.C.); grfleming@lbl.gov (G.R.F.).
† University of Oregon.
‡ University of California, Berkeley; Lawrence Berkeley National Laboratory.

10.1021/jp047015u CCC: $27.50
Published on Web 11/25/2004

of electronic population between the chromphores, which has not been observed to date in the intact light-harvesting antennas,[15,16] the emission anisotropy decays to its asymptotic value in just a few vibrational periods.

A surface-crossing picture of coherent electronic energy transfer helps illuminate the coordinated nature of the "donor" and "acceptor" vibrations, especially in the case of weak energy-transfer coupling. The in-phase behavior of both the vibrational motion and the parallel and perpendicular emission from a chromophore pair with equal site energies can be predicted from the symmetric location of the intersection between donor-excited and acceptor-excited electronic potential energy surfaces. In the case of downhill excitation transfer, surface crossing from the donor-excited to the acceptor-excited potential surface occurs most efficiently in certain configurations where the two vibrational modes have different coordinate values. Interestingly, we find that the resulting difference in the phase of motion between vibrational wave packets on the two surfaces does not necessarily lead to a phase difference between the quantum beats in the parallel and perpendicular emission.

Quantum beats with vibrational periodicity, in phase between parallel and perpendicular emission, are also observed in the presence of strong energy-transfer coupling. With short enough excitation and detection pulses, these appear superimposed on higher-frequency oscillations due to coherent back-and-forth excitation transfer; the electronic beats are *out of phase* between parallel and perpendicular emission, as we should expect. The strong coupling case is found to be distinguished additionally from the weaker-transfer case by the occurrence of significant amounts of electronic interference in excitation and emission. Our analytical expression for the strong-transfer signal pinpoints the role of the emergent vibrational frequencies, distorted from those of the isolated chromophores, which govern adiabatic electronic energy transfer.

Although our dimer model differs in some significant respects from the multi-chromophore rings of bacterial light-harvesting antennas, we are nonetheless able to conclude that long-lived quantum beats born of vibrational coherence transfer and trapping can be a generic feature of energy transfer following vibrationally abrupt electronic excitation. In addition to rationalizing the otherwise counter-intuitive behavior of polarized emission from light-harvesting antennas, these findings suggest possible means of exerting external optical control over intermolecular energy transfer.

II. Theory

We consider a dimer complex whose Hamiltonian

$$H = |0\rangle H_0\langle 0| + |1\rangle H_1\langle 1| + |1'\rangle H_{1'}\langle 1'| + |2\rangle H_2\langle 2| + J\{|1'\rangle\langle 1| + |1\rangle\langle 1'|\} \quad (1)$$

comprises four electronic levels: $|0\rangle = |g_a g_b\rangle$ with both molecules unexcited, $|1\rangle = |e_a g_b\rangle$ with the "donor" excited, $|1'\rangle = |g_a e_b\rangle$ with the "acceptor" excited, and $|2\rangle = |e_a e_b\rangle$ with both molecules excited.[17] The corresponding nuclear Hamiltonians

$$H_j = \frac{p_a^2}{2m} + \frac{p_b^2}{2m} + v_j(q_a, q_b) \quad (2)$$

with potential energy surfaces

$$v_0 = \frac{m\omega^2}{2}(q_a^2 + q_b^2) \quad (3)$$

$$v_1 = \epsilon_1 + \frac{m\omega^2}{2}((q_a - d)^2 + q_b^2) \quad (4)$$

$$v_{1'} = \epsilon_{1'} + \frac{m\omega^2}{2}(q_a^2 + (q_b - d)^2) \quad (5)$$

$$v_2 = \epsilon_2 + \frac{m\omega^2}{2}((q_a - d)^2 + (q_b - d)^2) \quad (6)$$

govern the motion of one intramolecular vibration in each chromophore. As shown in Figure 1, the equilibrium position of a vibrational mode is displaced by a distance d when the host molecule is electronically excited. The site energy of the two-exciton state is typically $\epsilon_2 \cong \epsilon_1 + \epsilon_{1'}$.[18-21]

Instead of calculating the time- and frequency-gated spontaneous emission signal, we will determine the (very similar) emission stimulated by direct interaction with a probe pulse. In the presence of pump (C) and probe (D) laser pulses, the time-dependent Hamiltonian becomes

$$H(t) = H + V_C(t) + V_D(t) \quad (7)$$

where

$$V_I(t) = -\hat{\boldsymbol{\mu}}\cdot\boldsymbol{E}_I(t); \quad I = C,D \quad (8)$$

is the interaction with a laser pulse

$$\boldsymbol{E}_I(t) = \boldsymbol{e}_I A_I(t - t_I)\cos(\Omega_I(t - t_I) + \Phi_I) \quad (9)$$

of specified polarization, envelope, arrival time, carrier frequency, and phase.[22-24] We use Gaussian pulses with $A_I(t) = A_I\exp(-t^2/2\sigma_I^2)$ and define the delay $t_d = t_D - t_C$. The electronic dipole operator

$$\hat{\boldsymbol{\mu}} = \boldsymbol{\mu}_a(|1\rangle\langle 0| + |2\rangle\langle 1'|) + \boldsymbol{\mu}_b(|1'\rangle\langle 0| + |2\rangle\langle 1|) + Hc \quad (10)$$

connects states whose exciton numbers differ by one. We assign transition dipoles of strength $\mu = \mu_a = \mu_b$ to both molecules.

If the donor (a) and acceptor (b) moments are nonparallel, energy transfer from one chromophore to the other following C-pulse excitation will alter the polarization of light emission stimulated by the D pulse. The pump pulse is taken to be near vertical resonance ($\Omega_C \approx v_1(q_a = q_b = 0)$) and the probe is significantly red-shifted (with $\Omega_D < \Omega_C$), so that the signal is dominated by stimulated emission (at the expense of excited-state absorption and ground-state bleaching). A straightforward perturbation theory analysis shows that the stimulated emission signal[25] can be expressed as

$$S(t_d) = \langle\psi_n|\langle 0|C^\dagger[-t_d]D^\dagger|0\rangle\langle 0|D[t_d]C|0\rangle|\psi_n\rangle \quad (11)$$

where $|\psi_n\rangle$ is the initially occupied vibrational eigenstate (with $H_0|\psi_n\rangle = E_n|\psi_n\rangle$), $[t_d] \equiv \exp(-iHt_d)$ is the free-evolution operator for the dimer complex, and C and D are pulse propagators

$$I = -i\int_{-\infty}^{\infty} d\tau[-\tau + t_I]V_I(\tau)[\tau - t_I] \quad (12)$$

We set $\hbar = 1$ throughout. Equation 11 is the squared norm of the nuclear probability amplitude in the electronic ground state, $\langle 0|D[t_d]C|0\rangle|\psi_n\rangle$, generated by pump excitation, free evolution, and probe de-excitation.[26] It has the same form as a short-pulse-gated spontaneous emission signal.[27,28] Since excited-state absorption and ground-state bleaching do not contribute to a time-gated emission signal (as measured, for example, by

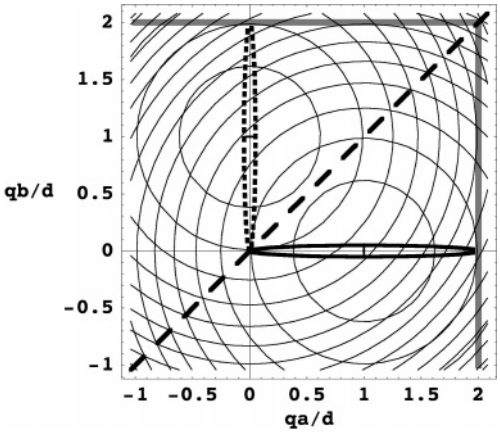

Figure 1. Contour plots of potential energy surfaces for the "donor-excited" electronic state, with its minimum at $(q_a,q_b) = (d,0)$, and the "acceptor-excited" state, with its minimum at $(0,d)$. The Franck−Condon point is at the origin, and the two excited-state potentials intersect along the diagonal in the case of equal site energies. The trajectories shown (drawn as narrow ellipses for clarity) are the spatial paths for wave packet motion following short-pulse excitation to the 1-state (solid) and an impulsive energy-transfer surface-crossing transition to the 1′-state (dotted). Vertical and horizontal gray bands locate the positions of emission resonance, for our chosen probe frequency, from the donor- and acceptor-excited states, respectively.

fluorescence up-conversion), eq 11 can be applied to the latter without the restrictions on pump and detection frequencies stated above.

The signal (11) is for a fixed spatial orientation of the energy-transfer complex. Through the pulse propagators, it depends on the laser polarizations, $\boldsymbol{e}_C$ and $\boldsymbol{e}_D$, relative to $\boldsymbol{\mu}_a$ and $\boldsymbol{\mu}_b$. A real sample will ordinarily consist of donor−acceptor pairs of a given structure randomly oriented in space. Using Euler angles, the signal from such a sample can be obtained by averaging (11) over lab-frame orientations while maintaining a fixed geometry within the complex. For the case $\boldsymbol{e}_C = \boldsymbol{e}_D$, this procedure leads to a parallel-emission signal

$$S_{||}(t_d) = \mu^4\left\langle \psi_n \middle| \left\langle 0 \middle| \frac{1}{5}pppp + \frac{\cos\alpha}{5}(p'ppp + pp'pp + ppp'p + pppp') + \frac{(1+2\cos^2\alpha)}{15}(p'p'pp + p'pp'p + p'ppp' + pp'p'p + pp'pp' + ppp'p') + \frac{\cos\alpha}{5}(pp'p'p' + p'pp'p' + p'p'pp' + p'p'p'p) + \frac{1}{5}p'p'p'p' \middle| 0 \right\rangle \middle| \psi_n \right\rangle \quad (13)$$

When the pump and probe polarizations are perpendicular, we obtain

$$S_{\perp}(t_d) = \mu^4\left\langle \psi_n \middle| \left\langle 0 \middle| \frac{1}{15}pppp + \frac{\cos\alpha}{15}(p'ppp + pp'pp + ppp'p + pppp') + \frac{(3\cos^2\alpha - 1)}{30}(p'p'pp + p'pp'p + pp'pp' + ppp'p') + \frac{(2-\cos^2\alpha)}{15}(p'ppp' + pp'p'p) + \frac{\cos\alpha}{15}(pp'p'p' + p'pp'p' + p'p'pp' + p'p'p'p) + \frac{1}{15}p'p'p'p' \middle| 0 \right\rangle \middle| \psi_n \right\rangle \quad (14)$$

α is the angle between donor and acceptor transition dipole moments, and $p = |1\rangle\langle 1|$ and $p' = |1'\rangle\langle 1'|$ are projection operators for the site-excited states. Equations 13 and 14 use a streamlined notation in which, for example, *pppp* stands for $c^\dagger p[-t_d]pd^\dagger|0\rangle\langle 0|dp[t_d]pc$, where c and d are *reduced pulse propagators* obtained from C and D by replacing all four $\boldsymbol{\mu}_I\cdot\boldsymbol{e}_I$ by unity. Calculation of the polarized emission through eqs 13 and 14 reduces to the task of constructing matrix representations of the free evolution operator and the reduced pulse propagators for a chosen set of chromophore-complex and laser pulse parameters.[29,30]

The various contributions to $S_{||}$ and $S_{\perp}$ can be described physically. The terms proportional to *pppp* or $p'p'p'p'$ report on the squared norm of wave packets prepared and detected on the same, donor-excited or acceptor-excited surface, respectively. Contributions proportional to $p'ppp' + pp'p'p$ involve the squared norm of an energy-transfer wave packet, prepared on one single-exciton surface and detected on the other; these terms will most clearly reveal any effects of vibrational coherence transfer. The first and fourth terms in the sum $p'p'pp + p'pp'p + pp'pp' + ppp'p'$ involve the *overlap* of a wave packet prepared and detected on the acceptor-excited surface with one excited to and de-excited from the donor-excited surface, whereas the second and third terms involve the overlap between two wave packets excited to one surface and de-excited from the other, but in reverse order. All four of these terms require electronic interference in absorption and emission and become small if this interference is turned off by poor overlap between the differing nuclear wave packets. The remaining contributions, which all vanish in the case of perpendicular transition dipole moments ($\alpha = \pi/2$), arise from overlaps between wave packets that have undergone differing orders (even or odd) of excitation transfer.[31]

The free evolution operator need only be determined within the one-exciton manifold spanned by $|1\rangle$ and $|1'\rangle$. We use a basis $\{|1\rangle|(n_a,n_b)_1\rangle,|1'\rangle|(n_a,n_b)_{1'}\rangle\}$ of zeroth-order (in J) eigenstates of the two-dimensional harmonic oscillator Hamiltonians governing the vibrations of both chromophores in the site-excited states.[32] The matrix elements of $H_{one} = pH_1 + p'H_{1'} + J(|1'\rangle\langle 1| + |1\rangle\langle 1'|)$ are written in terms of two-dimensional harmonic oscillator eigenenergies and products of translation-operator matrix elements, $\langle n'_a|D(\delta)|n_a\rangle$ and $\langle n'_b|D(\delta)|n_b\rangle$ (i.e. Franck−Condon overlaps). $D(\alpha) \equiv \exp(\alpha a^\dagger - \alpha^* a)$ and $\delta = d(m\omega/2)^{1/2}$ is the dimensionless mode displacement.[33] With site energies chosen from independent Gaussian distributions, we numerically diagonalize H_{one} to construct a matrix representation for $[t_d]_{one} = \sum_\eta|\eta\rangle\exp(-iE_\eta t_d)\langle\eta|$ in terms of the eigenvectors and eigenvalues of the one-exciton Hamiltonian.

The derivation of eqs 13 and 14 tacitly assumes that the relative orientation of a laser pulse's polarization and a site transition moment alone determines the amplitude for excitation or de-excitation; energy transfer is neglected in calculating the effects of each pulse. For instance, a pump pulse perpendicular to the "acceptor" transition moment ($\boldsymbol{\mu}_b\cdot\boldsymbol{e}_C = 0$) is not allowed to populate state $|1'\rangle$. Mathematically, this corresponds to making the replacement $[t] \cong \sum_j|j\rangle\exp(-iH_jt)\langle j|$ inside the pulse propagators (but not elsewhere), an approximation that should be valid if J is not too large and the pulses are not too long. With this neglect of J and making the usual rotating-wave approximation, the matrix elements of the reduced pulse propagators can readily be evaluated.[34]

Vibrational coherence transfer enters the emission signals most directly through $pp'p'p$ and $p'ppp'$ terms in eqs 13 and 14. The first of these, for example, gives the squared norm of $\langle 0|d|1'\rangle\langle 1'|[t_d]|1\rangle\langle 1|c|0\rangle|\psi_n\rangle$, the wave packet formed in the

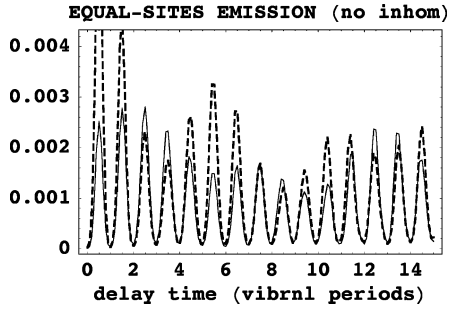

Figure 2. Orientationally averaged parallel (dashed) and perpendicular (solid) emission signals from an energy transfer complex with perpendicular transition moments and equal site energies. Excitation pulse is centered at the vertical transition energy and probe frequency selects for probability density at the outer turning point of either chromophore's vibration. Vertical axes in this and all subsequent polarized emission plots are in identical arbitrary units.

dimer's electronic ground state by "donor" excitation, coherent transfer to the "acceptor" during t_d, and stimulated emission. Figure 1 sketches the spatial path of a wave packet in the donor-excited state and one formed in the acceptor-excited state by energy transfer. If the site energies are equal, this process should contribute to in-phase vibrational quantum beats in the parallel and perpendicular emission signals. For the donor-excited and acceptor-excited potentials intersect along the diagonal in the equal-energy case, and the surface-crossing energy-transfer transition can occur with facility at the Franck−Condon point $q_a \approx q_b \approx 0$. A q_a-wave packet, launched in the donor by short-pulse excitation, will in turn launch an *in-phase* q_b-wave packet when amplitude is transferred to the acceptor-excited state during each brief return to the Franck−Condon region. The in-phase donor and acceptor wave packets will contribute to quantum beats of the same phase in the emission signal, because a probe pulse of given center frequency selects for probability density in state 1 within a certain range of q_a values and probability density in state 1′ within the same range of q_b values. Because the phase relationship between vibrational oscillations in the emission from different site states is related in this way to the dynamics of wave packet surface-crossing, coordinated quantum beats should be a ubiquitous feature of short-pulse-driven polarized emission from energy transfer complexes.[35]

III. Calculations (and Some More Theory)

We choose the ground state $|\psi_n\rangle = |(0,0)_0\rangle$ as the initial vibrational state in our calculations. Although ambient-temperature experiments[1] involve an average over thermally occupied levels, this choice is a natural starting point. In our computations, time is reckoned in vibrational periods, so there is no need to assign a value to the vibrational frequency $\omega = 2\pi/\tau_{vib}$. The donor and acceptor transition dipoles are taken to be perpendicular ($\alpha = \pi/2$).

A. Equal Site Energies and Weak Coupling. We focus first on a situation with fairly weak energy-transfer coupling, $J = 0.3\omega$, and larger Franck−Condon energy, $E_{FC} = m\omega^2 d^2/2 = 2.5\omega$ ($\delta = \sqrt{2.5}$). Figure 2 shows the orientationally averaged polarized emission signals from an equal-energy complex with no site inhomogeneity. Both pulses have a short duration $\sigma_C = \sigma_D = 0.1\tau_{vib}$. The pump is resonant with the vertical transition frequency, $\Omega_C = \bar{\epsilon}_1 + E_{FC}$, and the probe is red-shifted to $\Omega_D = \bar{\epsilon}_1 - 3E_{FC}$, to be resonant at the outer turning point of either vibrational coordinate. As expected from our description of coherence transfer, the quantum beats in the parallel and perpendicular emissions are in phase with each other. The decreasing difference in magnitude between parallel and perpendicular over 15 vibrational periods is evidence of population equalization due to excitation transfer.

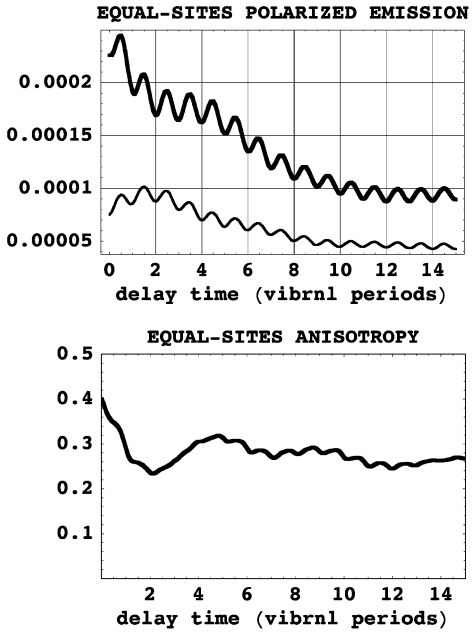

Figure 3. Top panel shows the parallel (heavy) and perpendicular (light) emission signals from an inhomogeneous collection of nearly equal site-energy dimers with the same system parameters as in Figure 2. Pulse frequencies are the same as previously, but pulse durations are lengthened slightly (vertical axis in arbitrary units). Bottom panel graphs the time-dependent anisotropy.

To model inhomogeneous broadening, we averaged signals from 1425 realizations of the chromphore complex having the two site energies randomly selected from independent Gaussian distributions with rms widths of 0.5ω and average values $\bar{\epsilon}_1 = \bar{\epsilon}_{1'}$. The pulse center frequencies are the same as before, but their durations are lengthened to $\sigma_C = 0.25\tau_{vib}$ and $\sigma_D = 0.5\tau_{vib}$ in order to approximate the typical time resolution of a fluorescence up-conversion experiment. Figure 3 plots the polarized emission and the anisotropy, $r(t_d) = (S_{||} - S_{\perp})/(S_{||} + 2S_{\perp})$. Excitation transfer from the initially excited chromophore accounts for the initial decrease (increase) in parallel (perpendicular) emission over several periods. The parallel and perpendicular emission signals exhibit in-phase oscillations at the vibrational frequency, which decease somewhat in amplitude over the course of some 15 periods. These in-phase vibrational quantum beats are similar to those observed in the up-conversion experiments on LH1.[1] The vibrational beats persist at least several times longer than the time-scale for energy transfer (inversely proportional to J), which is seen in the near-critically damped oscillation of the anisotropy. The anisotropy decays overall from an initial value of 0.4 to the range 0.25−0.27 during the last several periods calculated.[20,36−39] Vibrational-period oscillations are less prominent in the anisotropy, as is also observed experimentally. The long-time behavior of the emission anisotropy is addressed further in the Discussion section and Appendix A.

Calculations (not shown) using pulse durations much shorter than the inverse absorption bandwidth of this system have an initial emission anisotropy of 0.7. This high initial value−expected for a system of two chromophores with perpendicular transition dipoles[20]−decays to 0.4 within $\sim 0.2\tau_{vib}$, the time required for loss of overlap between the wave packets launched on the donor-excited and acceptor-excited potential surfaces. For longer pulses in this system with sizable Franck−Condon

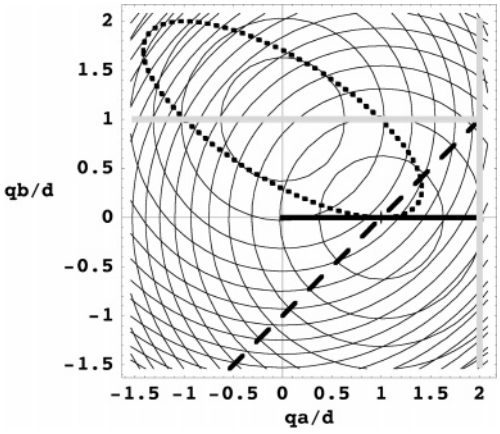

Figure 4. Donor-excited and acceptor-excited electronic potential energy surfaces along with their (dashed) line of intersection in the case of downhill transfer. Solid line shows the spatial path for wave packet motion after short-pulse excitation to the 1-state, while the elliptical dotted line is the path following a surface-crossing transition to the 1′-state. Lines of emission resonance from donor- and acceptor-excited states at our chosen probe−pulse frequency are shown as vertical and horizontal gray bands, respectively. Note shifted positions of acceptor emission relative to the equal-energy situation of Figure 1.

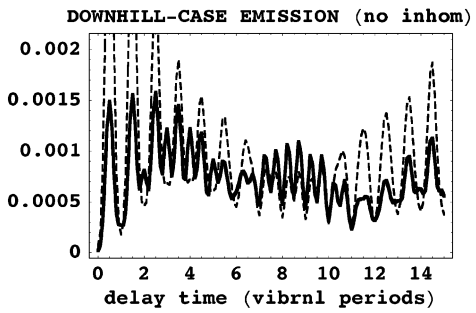

Figure 5. Parallel (dashed) and perpendicular (solid) emission signals in the downhill case. Excitation pulse is centered at the vertical transition frequency to the donor-excited potential and probe−pulse frequency selects for probability density at the outer turning point of the q_a-vibration in that state or the midpoint of q_b-vibration in the lower-energy acceptor-excited state. Vertical axis is in arbitrary units.

displacements, contributions from the terms in eqs 13 and 14 involving electronic interference in excitation and emission are found to be entirely negligible.

B. Unequal Site Energies and Weak Coupling. Although the equal-energy case is most relevant for energy transfer between similar chromophores in an LH1 complex, it is interesting to compare the situation of differing site energies.[40] Here vibrational wave packets in the higher-lying donor and lower-lying acceptor states remain coordinated but are no longer *in phase* with each other. As illustrated in Figure 4, surface-crossing energy-transfer transitions are expected to occur most strongly when the wave packet crosses the line $q_b = q_a - (\epsilon_1 - \epsilon_{1'})/m\omega^2 d$ where the potentials intersect. We examine the situation $\epsilon_{1'} = \epsilon_1 - 2E_{FC}$, in which the intersection passes through the $(q_a,q_b) = (d,0)$ minimum of the donor-excited potential. This case would produce maximal Förster overlap between acceptor absorption and donor fluorescence from a fully vibrationally relaxed state.

Figure 5 plots the emission signals from a single realization of the downhill dimer. As before, the transition moments are perpendicular, but $E_{FC} = 2.0\omega$ ($\delta = \sqrt{2.0}$) and $J = 0.2\omega$. The center frequencies are $\Omega_C = \bar{\epsilon}_1 + E_{FC}$ and $\Omega_D = \bar{\epsilon}_1 - 3.0E_{FC}$, and the pulse durations are $\sigma_C = \sigma_D = 0.1\tau_{vib}$. We again observe an initial decrease (increase) in magnitude of the parallel

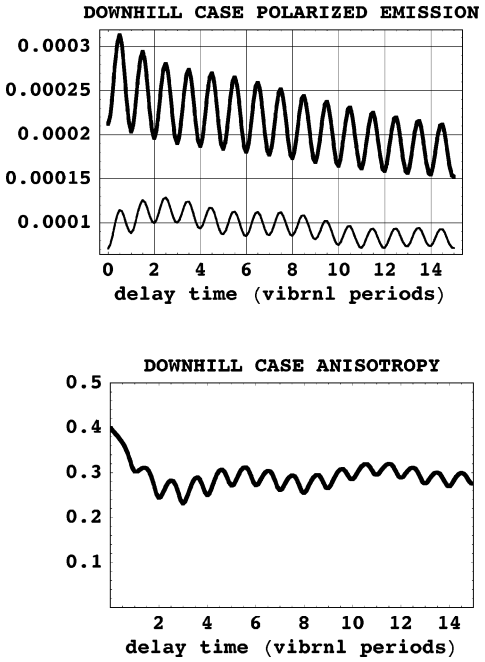

Figure 6. Top frame shows the parallel (heavy) and perpendicular (light) signals from an inhomogeneous collection of dimers in the downhill case. Other parameters are the same as in Figure 5, except that pulses are slightly longer (units on vertical axis are arbitrary). Bottom frame plots the time-dependent anisotropy.

(perpendicular) emission signal resulting from donor-to-acceptor energy transfer. The main sequence of quantum beats in the parallel emission signal has a period $\sim\tau_{vib}$ and is phased consistently with detection at the outer turning point of q_a. The perpendicular emission exhibits a series of beats in-phase with the main sequence from parallel emission and an additional series of *out-of-phase* peaks. At intermediate times, the parallel signal also shows several out-of-phase emission bursts.

Both series of beats in the perpendicular emission can be understood by considering the wave packet trajectories and the location of the detection window for acceptor-state emission. From Figure 4 we see that out-going and in-coming donor-excited wave packets will launch daughter acceptor-excited packets which follow an elliptical path in counterclockwise and clockwise directions, respectively. Due to the lower site energy of the acceptor, the probe pulse now selects for emission near $q_b = d$, rather than at the outer turning point. Thus the first pass through the acceptor probe window of a (counterclockwise) daughter wave packet launched by an out-going donor and the second pass of a (clockwise) daughter launched by an incoming donor packet should both contribute to emission bursts in-phase with the main sequence of parallel emission beats. Conversely, the second pass of the counterclockwise packets and the first pass of the clockwise packets contribute to emission beats that are out of phase with the main parallel sequence.

Figure 6 shows signals from a collection of 1199 downhill-transfer complexes with site energies chosen from independent Gaussian distributions of 0.4ω rms width. The Hamiltonian parameters and pulse frequencies are otherwise the same as for Figure 5, but $\sigma_C = 0.2\tau_{\rm vib}$ and $\sigma_D = 0.4\tau_{\rm vib}$. A steady decrease in the cycle-averaged parallel emission signal is observed, along with an increase over the first several periods in the perpendicular emission. A sequence of quantum beats of period $\tau_{\rm vib}$ phased consistently with probe detection at the outer turning point of the donor entirely dominates the parallel emission, and quantum beats in phase with this progression also dominate the perpendicular emission. The beats in both emission components

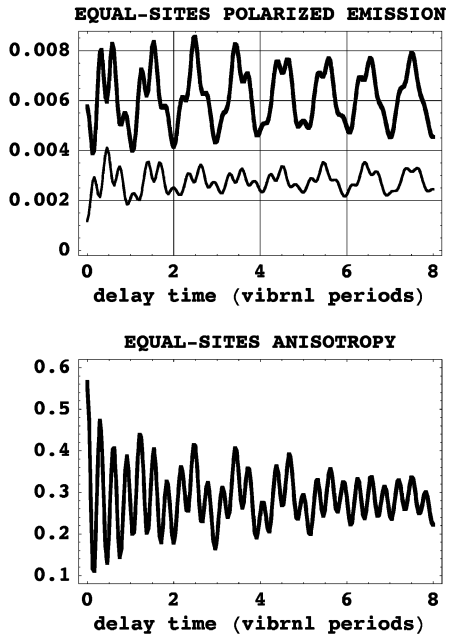

Figure 7. Top panel shows the parallel (heavy) and perpendicular (light) time-resolved emission from an inhomogeneous collection of nearly equal site-energy dimers with strong energy-transfer coupling. Vertical axis is in arbitrary units. See text for system and pulse parameters. Bottom panel plots the anisotropy.

are sharper than those in Figure 3 because of the smaller J, the decreased inhomogeneity, and the shorter pulses. The smaller out-of-phase quantum beats seen in the perpendicular emission of Figure 5 are washed out by the inhomogeneous broadening. As a result, the time-resolved emission anisotropy in the bottom of Figure 6 is surprisingly similar to the equal-energy case. The anisotropy decays from 0.4 to a long-time value slightly higher than for equal site energies. The damped oscillation due to back-and-forth energy transfer is less evident here, but the anisotropy shows more prominent vibrational quantum beats. As with previously calculated time-resolved emission signals from a one-dimensional electron-transfer model,[41] the emission dynamics from this downhill complex cannot be interpreted as arising solely from electronic population transfer.

C. Strong Coupling Case. The LH1 anisotropies measured by Bradforth et al. decayed biphasically from 0.4 to ~0.07 with time constants of 110 and ~400 fs.[1] Thus, energy transfer is more rapid than both the damping time, 450 fs, *and the period*, 312 fs, of the quantum beats observed in the polarized emission. Those and other[2] data indicate that the energy-transfer coupling strength in the light-harvesting complex exceeds the vibrational frequency itself and not just its damping rate. Evidence for strong coupling in LH1 is in keeping with the advantage it should confer by speeding the transport of electronic excitation to the reaction center and allowing less time for competing processes.

1. Numerical Results. Figure 7 shows calculated signals from a collection of equal-site dimers with stronger coupling, $J = 1.5\omega$, and smaller displacements, $E_{FC} = 0.5\omega$. The width of the site-energy distributions is 1.2ω (1364 realizations) and the pulses are short enough ($\sigma_C = 0.08\tau_{\text{vib}}$ and $\sigma_D = 0.12\tau_{\text{vib}}$) to justify neglect of energy transfer during pulse action. Center frequencies are $\Omega_C = \bar{\epsilon}_1 + E_{FC}$ and $\Omega_D = \bar{\epsilon}_1 - 3.0E_{FC}$. In the polarized emission, vibrational quantum beats are accompanied by higher-frequency oscillations corresponding to electronic excitation cycling. Although the vibrational beats are again in phase between parallel and perpendicular, the electronic oscillations in the two cases are out of phase. The former behavior is consistent with a role for vibrational coherence transfer, whereas the latter manifests the precessional transfer of excited-state population from and to the initially excited chromophore.[37,20] We shall see that electronic energy can also be transferred in this case as the site-character of the one-exciton eigenstates adiabatically follows a changing nuclear configuration.

2. Analytical Treatment. With strong coupling, $2J \gg \omega$, and small vibrational displacements, electronic excitation is transferred so quickly from site to site that the nuclear degrees of freedom have less time to respond than their natural time scale of motion.[11,42] The resulting adiabaticity of the nuclear motion enables a detailed analysis of the time-dependent polarized emission, which is summarized here and in Appendix B.

One diagonalizes the single-exciton electronic Hamiltonian

$$H_e(q_a,q_b) = v_1 p + v_{1'} p' + J(|1'\rangle\langle 1| + |1\rangle\langle 1'|) \qquad (15)$$

to obtain the eigenstates

$$|s(q_a,q_b)\rangle = |1\rangle\xi_s(q_a,q_b) + |1'\rangle\xi'_s(q_a,q_b) \qquad (16)$$

with $s = +$ or $-$, and the corresponding eigenenergies $U_+(q_a,q_b)$ and $U_-(q_a,q_b)$. Notice that the one-exciton eigenstates (and hence their transition moments to the electronic ground state) depend on nuclear configuration through the expansion coefficients in eq 16.

When $2J \gg E_{FC}$, a harmonic expansion of the adiabatic potentials becomes appropriate, and in terms of the normal coordinates $Q = (q_a + q_b)/2$ and $q = q_b - q_a$, these can be expressed as $U_s(Q,q) = V_s(Q) + v_s(q)$, where

$$V_s(Q) = \epsilon + sJ + \frac{M\omega^2}{2}\left(Q - \frac{d}{2}\right)^2 + \frac{M\omega^2 d^2}{8} \qquad (17)$$

$$v_s(q) = \frac{\mu\omega_s{}^2 q^2}{2} \qquad (18)$$

with $M = 2m$, $\mu = m/2$, and the difference-mode frequencies

$$\omega_s = \omega\sqrt{1 + 2s\lambda d}$$

where $\lambda \equiv E_{FC}/2Jd$. We have specialized to equal site energies $\epsilon_1 = \epsilon_{1'} = \epsilon$. Figure 8 shows the adiabatic potential surfaces $U_+(Q,q)$ and $U_-(Q,q)$. In these diagrams, Q increases diagonally and q does so anti-diagonally. The average-mode potentials $V_+(Q)$ and $V_-(Q)$ are simply vertically separated by $2J$ and correspond to the same frequency as the monomer vibrations. $v_+(q)$ and $v_-(q)$ have slightly higher and slightly lower frequencies (U_+ and U_- are more and less V-shaped along the anti-diagonal), respectively, than in the uncoupled monomers. Also shown are the curves of emission resonance from each adiabatic potential for the probe frequency used in our calculations. Due to the coordinate dependence of the adiabatic transition dipole moments, the wave packets prepared by short-pulse excitation on the two surfaces need not be centered at the ground-state equilibrium position.

Through second order in λ, the site coefficients of the electronic eigenstates are

$$\xi_s{}^{(j)}(q) = \frac{1}{\sqrt{2}}\left(s^{j+1} - (-s)^j\lambda q - \frac{s^{j+1}\lambda^2}{2}q^2\right) \qquad (19)$$

where $j = 1$ (2) identifies the unprimed (primed) coefficient.

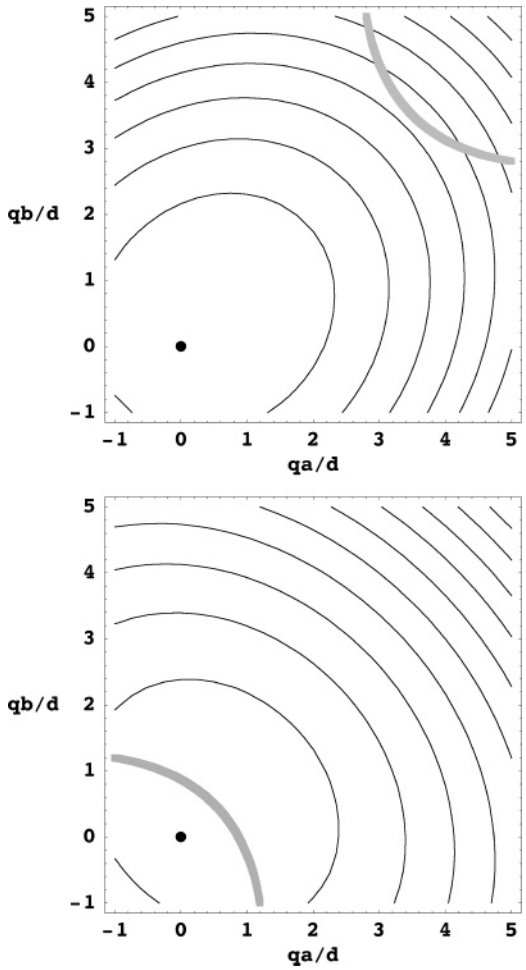

Figure 8. Contour plots of the harmonic upper (U_+, above) and lower (U_-, below) one-exciton adiabatic electronic potential energy surfaces in the case of strong coupling. $J = 1.5\omega$ and $E_{FC} = 0.5\omega$. Black dot at the origin indicates Franck−Condon point. Dark gray curves are loci of emission resonance for the probe frequency used in our calculations.

Since the $\xi_s^{(j)}$ depend only on q, the difference-mode serves as the "reaction coordinate" for adiabatic electronic energy transfer.[43−45] Within an adiabatic approximation that neglects transitions between $|+(q)\rangle$ and $|-(q)\rangle$ induced by motion along q, we can express the vibronic eigenstates $|s(\hat{q})\rangle|N\rangle|n_s\rangle$ ($N,n_s = 0,1,2\cdots$), in terms of displaced ($|N\rangle$) or squeezed ($|n_s\rangle$) vibrational wave functions from the electronic ground state. The corresponding eigenenergies are

$$E_{s,N,n_s} = \epsilon + sJ + M\omega^2 d^2/8 + \omega(N + 1/2) + \omega_s(n_s + 1/2) \tag{20}$$

It becomes a straightforward task to determine the polarized emission signals *through second order in* λ. With a vibrationally abrupt pump and a probe no longer than $\sim 1/2J$, the signal takes the form

$$S(t_d) = \kappa \sum_{s,s'} G_{s's}(t_d) g_{s's}(t_d) \tag{21}$$

where κ is proportional to the product of pump and probe pulse areas, and G and g depend on the average-mode and difference-mode dynamics, respectively. Expressions for the elements of G and g are given in Appendix B. The probe frequency dependence of the signal is carried by G, while orientational effects reside in g. Terms in eq 21 for which s equals s' involve absorption to and emission from a single adiabatic electronic state, and those with different s and s' account for electronic interference in absorption and emission. The signal can be averaged over the spatial orientation of the complex, as was done for eqs 13 and 14 (see Appendix B).

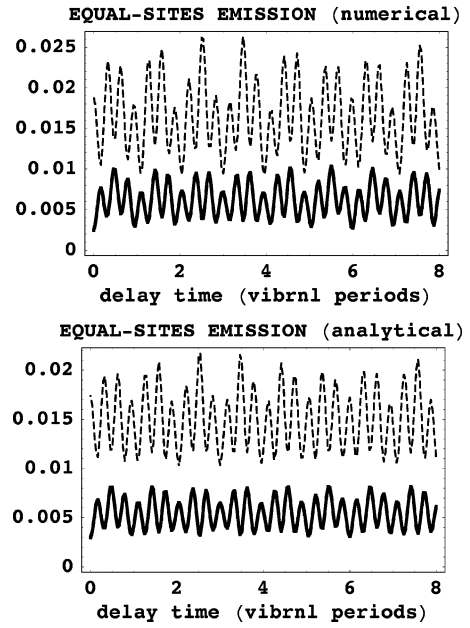

Figure 9. Upper (lower) panel shows numerical (analytical) polarized emission signals from a strongly coupled dimer with identical site energies. Dashed (solid) curve gives parallel (perpendicular) emission. See text for parameters. Both vertical axes are in the same arbitrary units.

Figure 9 compares numerical and analytical emission signals from an equal-site dimer with strong coupling. Parameters are the same as in Figure 7, except that the site energies are strictly equal and the pulse durations are $\sigma_C = 0$ and $\sigma_D = 0.06\tau_{vib}$.[46] The numerical and analytical results agree in detail, with both exhibiting electronic oscillations anti-phased between the parallel and perpendicular on an envelope of in-phase vibrational oscillations. The numerical and analytical plots use the same arbitrary scale, and the difference in signal intensity comes from our neglect of energy transfer during pulse action in the former and the adoption of adiabatic, harmonic, and semiclassical Franck−Condon approximations in the latter. These differences became less pronounced with shorter probe pulses and more pronounced for larger λd (calculations not shown).

IV. Discussion

Our calculations support vibrational coherence transfer and related processes to be discussed in this section as the likely underlying causes for the previously puzzling behavior of the quantum beats observed in time-resolved polarized emission signals from photosynthetic light-harvesting antennas. Most pertinently for fluorescence up-conversion data from LH1,[1] in the case of an equal site-energy dimer, coherence transfer is seen to contribute to in-phase quantum beats at the vibrational frequency in both parallel and perpendicular emission traces that outlive the decay of the anisotropy due to electronic population exchange between the donor and acceptor molecules. Coherence transfer occurs in such a way that the intramolecular donor and acceptor vibrations, coordinated by the nearly impulsive surface-crossing energy transfer process, are precisely *in phase* with each other. The in-phase vibrations in excited donor and excited acceptor molecules of the equal-sites dimer give rise to in-phase oscillations in the calculated parallel and

perpendicular time-gated emission signals similar to those observed in LH1.

The process of coherence transfer was previously identified as a feature of the dynamics in abruptly excited and slowly relaxing electron-transfer systems.[47] That study also found that vibrational coherence could be generated in an initially thermal state if the coupling was similar in strength to the vibrational frequency. The coherences of interest in that work were transferred between pairs of eigenstates of a single-mode subsystem due to its interaction with a surrounding medium. Our usage is related, but refers specifically to coherences transferred between different intramolecular vibrational modes by the energy transfer process itself, rather than as a consequence of relaxation. Examples of coherence transfer have been seen in pump−probe experiments on Iodine in rare-gas matrixes,[48] and−with evidence for a temporally decreasing vibrational period−in femtosecond stimulated emission pumping spectra of I_2^- in a Ar and CO_2 clusters.[49] Earlier examples of vibrational coherence transfer from reactants to products include those observed by two-color pump−probe measurements on the $I_3^- + h\nu \rightarrow I_2^- + I^*$ photodissociation process[50] and by transient absorption experiments on 11-cis + $h\nu$ → all-trans photoisomerization in the retinal chromophore of the rhodopsin visual pigment.[51]

A recent generalization of Förster-Dexter excitation transfer theory to account for unrelaxed vibrations at short times[52] deals in a more general way with some of the questions addressed in the present study. Jang, Jung, and Silbey (JJS) derived an expression for an excitation transfer *rate*−second order in the coupling element *J*, which incorporates the effects of nonequilibrium intra-chromophore vibrations through a time-dependent overlap between donor emission and acceptor absorption spectra. Their explicit calculations assumed distinguishable donors and acceptors and specialized to certain continuous spectral densities of independent (donor and acceptor) "bath" vibrations; the results show time-varying reaction rates with weakly oscillatory components on the vibrational time-scale. Although the time-resolved polarized emission does not depend solely on the changing acceptor population in general, the variations in transfer rate that JJS predict, governed by an oscillatory overlap between donor emission and acceptor absorption, may in effect already have been observed in LH1.

It is important not to oversimplify the interpretation of quantum beats in the polarized emission signals by directly equating vibrational-period oscillations in the parallel signal with coherences in the donor-excited state and oscillations in the perpendicular signal with vibrational coherence transfer. Donor emission contributes primarily, but not solely, to the parallel signal. In a similar way, acceptor emission does not contribute exclusively to the perpendicular signal. Quantitatively from eq 13, the $pppp + p'p'p'p'$ term, which accounts for absorption and emission from the same chromophore, contributes to $S_{||}$ in a ratio of 1/5 to 1/15 with the $pp'p'p + p'ppp'$ term, which describes absorption and emission from different chromophores (assuming perpendicular transition moments). From eq 14 on the other hand, there is a ratio of 1/15 to 2/15 between the $pppp + p'p'p'p'$ and $pp'p'p + p'ppp'$ contributions to $S_\perp$.[53]

The terms describing absorption and emission from different molecules should most directly manifest vibrational coherence transfer. But as population cycles between donor and acceptor, *coherence back-transfer* can alter the vibrational coherence in the donor-excited state as well. Coherence back-transfer would thus affect both parallel and perpendicular signals through terms involving absorption and emission from the same chromophore.

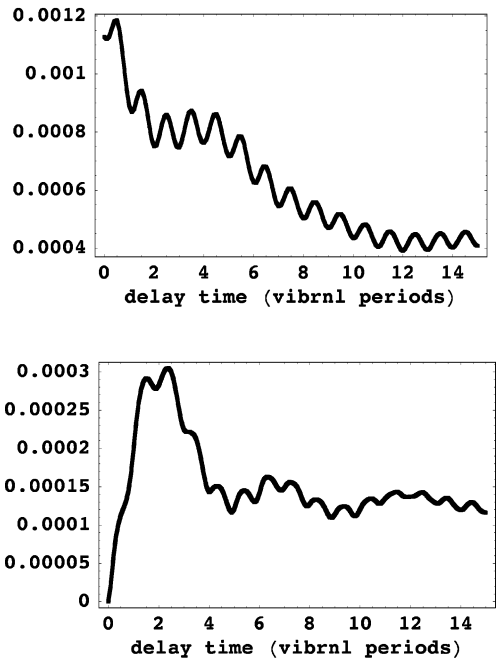

Figure 10. Major contributions to emission signals of Figure 3. Top panel shows $pppp + p'p'p'p'$ term, which describes absorption to and emission from the same site-excited state. Bottom panel displays $pp'p'p + p'ppp'$, which accounts for excitation transfer and vibrational coherence transfer between the site states. Vertical axes in identical arbitrary units. These are the only significant contributions to $S_{||}$ and $S_\perp$ in this system.

The upper panel of Figure 10 shows the $pppp + p'p'p'p'$ term for the collection of weakly coupled equal-site dimers considered in Figure 3, and the lower panel plots the $pp'p'p + p'ppp'$ term for the same system. Near $t_d \approx 10\tau_{vib}$ the quantum beats in the former are of range $osc \approx 6.4 \times 10^{-5}$ and those in the latter are of range $osc' \approx 1.5 \times 10^{-5}$, in the same arbitrary units. *osc′* results entirely from vibrational coherence transfer, and the *back-transfer* of vibrational coherence may also contribute to *osc* at this delay time. We can obtain a lower bound for the effects of coherence transfer by ignoring its contribution to *osc* and estimating that $2osc'/(osc+2osc')$, or about one-third, of the quantum beat amplitude in $S_\perp$ results from vibrational coherence transfer.

Even after coherence transfer and back-transfer have operated extensively, along with depletion of the donor-excited state, there may remain vibrational coherences which are effectively *trapped* in the donor. Some vibrational levels in each site state have negligibly small Franck−Condon overlaps with isoenergetic levels in the other state, and amplitude in both sets of levels remains largely unaffected by excitation transfer. The superposition among donor-excited vibrational levels prepared by a pulse may include some of these trapped states or may have negligible amplitude in the crossing region due to local destructive interference among untrapped site vibrational eigenstates. The resulting vibrational coherence would make a contribution to $pppp + p'p'p'p'$ that persists more-or-less indefinitely in the absence of relaxation. In wave packet terms, these trapped coherences can be viewed as forming a wave packet that executes harmonic motion between $(q_a,q_b) \approx (0, -\beta)$ and $(2d,\beta)$ in the donor-excited state, where β is a small displacement. Such a wave packet would be largely immune from energy transfer because it never crosses the line $v_1 = v_{1'}$.

It is worth pointing out that under certain circumstances, different contributions to the pump−probe emission signal should be experimentally isolable with some choice of pulse

polarizations. As demonstrated above,[30] the signal for an arbitrary relative polarization of pump and probe can be written as a linear combination of $S_{||}$ and $S_{\perp}$; it is enough to ask whether a given contribution to the signal can be obtained by adding together these two "base signals" with some relative weights. For the system in Figure 3 featuring relatively strong electron-vibration coupling, all signal contributions involving electronic interference between sites are tiny. As a result we see, for instance, that the combination $S_{||} - 3S_{\perp}$ is proportional to the $pp'p'p + p'ppp'$ term plotted in the bottom panel of Figure 10.[54]

Bacterial light harvesting antennas are multi-chromophore complexes of broken elliptical shape, rather than dimers, so our calculations cannot be regarded as direct simulations of the LH1 data.[55,56] However, the simple dynamics entering the calculated polarized emission signals suggests that coordinated vibrational beats arising from coherence transfer and trapping should be a ubiquitous feature of light emission from impulsively excited multi-chromophore systems with surface-crossing dynamics.[57]

Our calculated long-time anisotropy for the weakly coupled equal-sites dimer (~0.26), differs from that observed in LH1 (~0.1).[1] This difference results from our neglect of vibrational relaxation, which is slower than electronic energy transfer and electronic inhomogeneous dephasing. Appendix A demonstrates how including vibrational relaxation[20,43,58−61] will lead to the correct limiting anisotropy. The inclusion of multiple vibrational modes in time-dependent nonlinear optical signals from energy-transfer complexes, already studied for a variety of linear measurements,[62] should be a topic for further investigation.

Phthalocyanine dimer and trimer complexes have been studied as models for photosynthetic energy transfer, and their various electronic excitations elucidated.[63] Two-color photon echo experiments on coupled phthalocyanine dimers[64] support many aspects of Ishikawa's analysis and reveal ~160 cm^{-1} quantum oscillations−attributed to molecular vibration−whose phase was seen to differ by π from those observed in one-color experiments. In light of the more complicated electronic structure of these dimers, which feature excited states of mixed Frenkel-exciton and charge-transfer character, it will be interesting to determine whether the dynamics underlying the quantum beats is related to that considered here.

We reported calculations of the emission dynamics from a dimer with a site energy difference of $2E_{FC}$, corresponding to the "barrierless" case for Förster transfer. Here the donor-mode and acceptor-mode vibrations are still coordinated by impulsive energy transfer, but differ by 90° in their phase of motion. In the presence of broadened site energies, this phase shift did not alter the in-phase relationship between parallel and perpendicular emission beats. Our choice of probe center frequency was special, however, selecting for vibrational probability density at the outer turning point of the donor-mode vibration and halfway between inner and outer acceptor-mode turning points. For an arbitrary probe frequency, the donor- and acceptor-emission vibrational beats would be phase shifted with respect to each other.[65] In contrast to the equal-energy situation, vibrational coherence trapping would not be expected to operate effectively in the downhill case, because there is no way of leaving behind a localized residual wave packet in the donor-excited-state whose motion avoids the potential energy intersection line. A delocalized quasi-stationary vibrational distribution with a node of probability density along the intersection line could remain trapped in this case, however.

Vibrational coherence transfer also occurs in the strong-coupling case most directly pertinent to LH1. Figure 11 shows the $pppp + p'p'p'p'$ and $pp'p'p + p'ppp'$ terms for the strongly coupled dimer complex of Figure 7. Both terms display prominent vibrational-period oscillations (with those in the $pp'p'p + p'ppp'$ terms resulting entirely from coherence transfer) along with higher-frequency electronic oscillations. Also shown is the $p'p'pp + ppp'p' + p'pp'p + pp'pp'$ contribution, which accounts for electronic interference between sites in absorption and emission. Similar in magnitude to $pppp + p'p'p'p'$, the electronic interference term also shows vibrational-period quantum beats. It does not exhibit electronic oscillations because the portions with $(p'pp'p + pp'pp')$ and without $(p'p'pp + ppp'p')$ excitation transfer are roughly proportional to $1 - \cos 2Jt_d$ and $1 + \cos 2Jt_d$, respectively, and the cosines cancel.

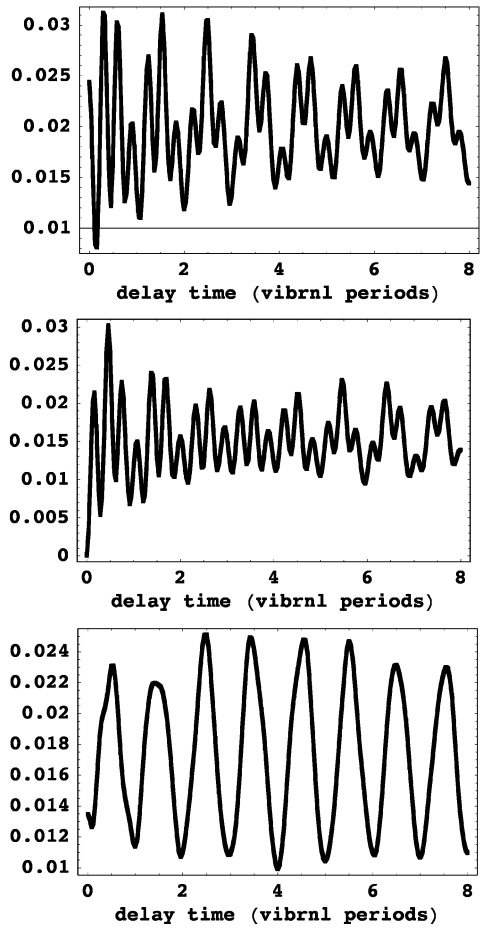

Figure 11. Contributions to polarized emission of Figure 7 with equal site energies and strong coupling. Top: $pppp + p'p'p'p'$. Middle: $pp'p'p + p'ppp'$. Bottom: $p'p'pp + ppp'p' + p'pp'p + pp'pp'$ term describing electronic interference between *sites*. Last quantity is nonnegligible in this strongly coupled system with small vibrational displacements. All vertical axes in identical arbitrary units.

Our analytical treatment of the strong-coupling case identifies the emergent vibrational frequencies ω_+ and ω_- given below eq 18. Alluded to in early descriptions of strongly coupled energy transfer,[11] these new "vibrational" frequencies are a limiting illustration of the emergence of new vibronic eigenenergies that occurs whenever energy-transfer coupling significantly distorts the adiabatic potentials.[66] The elements of $G_{s's}(t_d)$ (eq B2) with $s' \neq s$ contribute to interference between the *adiabatic* electronic states in absorption and emission and carry a $2J$ oscillation. In the signal (21) this bare electronic oscillation combines with vibrational difference frequencies in $g_{s's}(t_d)$ (eqs B5, B6, and B8) to produce oscillations at $2J + (\omega_+ - \omega_-)/2$, $2J + (3\omega_+ - \omega_-)/2$, $2J + (\omega_+ - 3\omega_-)/2$, $2J + (5\omega_+ - \omega_-)/2$, $2J + (\omega_+ - 5\omega_-)/2$, $2J + (3\omega_+ - 3\omega_-)/2$, and $2J + (5\omega_+ - 5\omega_-)/2$. In the $s' = s$ contributions, purely "vibrational"

oscillations occur at frequencies ω_+, ω_-, $2\omega_+$, and $2\omega_-$ in addition to ω (see eq B8). These new vibrational frequencies govern the wave packet motion that gives rise to adiabatic excitation transfer. Shifted frequencies of this kind may account for some of the spectral density seen below and above 105 cm^{-1} in transient absorption measurements on LH1 by Monshouwer et al.[67]

V. Conclusion

In addition to resolving a perplexing feature of the light-emission from short-pulse excited photosynthetic antenna complexes, our proposed explanation (and the experimental data themselves) points to an influential role for molecular and intermolecular vibrations in short-time electronic energy transfer.[68] Beyond emphasizing that a detailed account of Franck−Condon active or frequency-shifted vibrations, including their coherent excitation and subsequent damping, will be an important ingredient in an accurate portrayal of photosynthetic and other electronic energy transfer dynamics, these findings open the prospect of using external control over molecular vibrations as a means of influencing the transport among coupled chromophores of higher-energy electronic excitations. It will be interesting to discover to what extent control strategies designed in that way illuminate or provide alternatives to random-search methods, which have already met with some success in governing the time-course of photosynthetic energy transfer.[69]

Appendix A. Long-Time Anisotropy

The effects of vibrational relaxation could be incorporated by including the nuclear degrees of freedom of a surrounding medium. Prior to excitation, the state is $|0\rangle|\psi\rangle = |0\rangle|(0,0)_0\rangle|bth\rangle$, in which $|(0,0)_0\rangle$ and $|bth\rangle$ are vibrational eigenstates of the chromophore pair and the surrounding medium, respectively (compare Section II). The orientationally averaged signal expressions (13) and (14) would then comprise terms of the form

$$\langle bth|\langle(0,0)_0|\langle 0|c^\dagger p^{(i)}[-t_d]p^{(j)}d^\dagger|0\rangle\langle 0|dp^{(k)}[t_d]p^{(l)}c|0\rangle |(0,0)_0\rangle|bth\rangle \quad \text{(A1)}$$

where each superscripted projection operator denotes either p or p', and c and d are the reduced pulse propagators. The free evolution, $[t_d]$, is governed by a Hamiltonian which includes both dimer and bath degrees of freedom.

A vibrationally abrupt pump pulse prepares the photoexcited state

$$p^{(l)}c|0\rangle|(0,0)_0\rangle|bth\rangle \cong \frac{i}{2}A_C\sigma_C\sqrt{2\pi}\mathrm{e}^{-i\Phi_C}p^{(l)}(|1\rangle + |1'\rangle)|(0,0)_0\rangle|bth\rangle = \frac{i}{2}A_C\sigma_C\sqrt{2\pi}\mathrm{e}^{-i\Phi_C}|(l)\rangle|(0,0)_0\rangle|bth\rangle \quad \text{(A2)}$$

In either case (p or p'), the propagated state ket

$$[t_d]p^{(l)}c|0\rangle|(0,0)_0\rangle|bth\rangle = \frac{i}{2}A_C\sigma_C\sqrt{2\pi}\mathrm{e}^{-i\Phi_C}\sum_\zeta|\zeta\rangle|bth_\zeta{}^{(l)}(t_d)\rangle \quad \text{(A3)}$$

is a sum of tensor products of one-exciton eigenstates of the dimer denoted by $|\zeta\rangle$ and time-dependent bath states specific to l and ζ. At t_d longer than some vibrational relaxation time, and with the assumption that system-bath interactions are weaker than the splittings between vibronic levels, the sum in eq A3 will be dominated by the term $|\zeta_0\rangle|bth_0{}^{(l)}(t_d)\rangle$, where $|\zeta_0\rangle \cong \{(|1\rangle|(0,0)_1\rangle - |1'\rangle|(0,0)_{1'}\rangle)\}/\{\sqrt{2}\}$ is the lowest-lying state in the case of equal site energies. This "ground-state dominance" occurs because there are *many* more states accessible to the high-dimensional bath with the full available energy $E_{FC} - E_{\zeta_0}$ than with any reduced allotment $E_{FC} - E_{\zeta>0}$. Having p- and p'-projected states both acquire the same general form does not violate unitary evolution, because the corresponding long-time bath states are essentially orthogonal: $\langle bth'_0(t_d)|bth_0(t_d)\rangle = 0$.

Using the resulting form (A3) for both bra and ket in eq A1 and ignoring any small effect of the probe−pulse propagator on the bath states, we find

$$\langle bth|\langle(0,0)_0|\langle 0|c^\dagger p^{(i)}[-t_d]p^{(j)}d^\dagger|0\rangle\langle 0|dp^{(k)}[t_d]p^{(l)}c|0\rangle \times |(0,0)_0\rangle|bth\rangle \cong \frac{\pi}{4}A_C{}^2\sigma_C{}^2\langle bth_0{}^{(i)}(t_d)|bth_0{}^{(l)}(t_d)\rangle \times \langle(0,0)_j|\langle(j)|d^\dagger|0\rangle\langle 0|d|(k)\rangle|(0,0)_k\rangle \quad \text{(A4)}$$

The long-time bath states for $i \neq l$ are effectively orthogonal, and the vibrational states $|(0,0)_j\rangle$ and $|(0,0)_k\rangle$ copied to the ground-state potential by the probe pulse should have little overlap if they come from different excited-state wells. Thus, the site-state indices in eq A1 must obey $i = l$ and $j = k$ in order to give a nonnegligible contribution at long times, and the nonvanishing terms (A1) should all take essentially the same value. The long-time anisotropy can be calculated from the resulting proportionalities

$$S_{||} \propto \frac{2}{5} + 2\frac{1 + 2\cos^2\alpha}{15} \quad \text{(A5)}$$

$$S_\perp \propto \frac{2}{15} + 2\frac{2 - \cos^2\alpha}{15} \quad \text{(A6)}$$

Whence

$$\frac{S_{||} - S_\perp}{S_{||} + 2S_\perp} = \frac{1}{10} + \frac{3}{10}\cos^2\alpha \quad \text{(A7)}$$

which gives 0.1 for $\alpha = \pi/2$ and 0.4 for $\alpha = 0$.

Appendix B. Adiabatic Analysis

$G_{s's}(t_d) = \langle av g_{s'}|av g_s\rangle$ in formula (21) is the inner product of time-dependent average-mode kets

$$|av g_s\rangle = \exp\{-c(\hat{Q} - Q_{Ds})^2\}\exp\left\{-it_d\left(\frac{\hat{P}^2}{2M} + V_s(\hat{Q})\right)\right\} \times \exp\left\{i\frac{d}{2}\hat{P}\right\}|N = 0\rangle \quad \text{(B1)}$$

in which $c = \sigma_D{}^2M^2\omega^4d^2/8$ and $Q_{Ds} \equiv (2/M\omega^2d)(\epsilon + sJ + M\omega^2d^2/4 - \Omega_D)$.[70] The wave packet (B1) is prepared by an abrupt pump pulse, propagated for t_d by the appropriate average-mode Hamiltonian, and dumped to the ground potential energy surface by a short probe. The wave function for the lowest-lying state of the average-mode Hamiltonian in either one-exciton level is $\langle Q|N = 0\rangle = (M\omega/\pi)^{1/4}\exp\{-(M\omega/2)(Q - d/2)^2\}$, and the translation operator $\exp\{id\hat{P}/2\}$ moves it to the Franck−Condon point, where its evolution begins. Since $\exp\{-it_d(\hat{P}^2/2M + V_s(\hat{Q}))\}\exp\{id\hat{P}/2\}|N = 0\rangle$ is a Glauber coherent state, its time development takes a compact form[33] which together with the short σ_D leads to

$$G_{s's}(t_d) \cong \sqrt{\frac{M\omega}{M\omega + c}} \exp\left\{ it_d J(s' - s) - 2c\left(\bar{Q}(t_d) - \frac{Q_{Ds'} + Q_{Ds}}{2}\right)^2 - \frac{c}{2}(Q_{Ds'} - Q_{Ds})^2 \right\} \quad \text{(B2)}$$

with $\bar{Q}(t_d) = d(1 - \cos\omega t_d)/2$.

The evaluation of $g_{s's}(t_d)$ in eq 21 is more involved. This term accounts for the polarization dependence of the signal. The terms with $s = s'$ involve adiabatic excitation transfer, which accompanies motion from a (q_a,q_b) configuration corresponding to "donor" excitation−one with $q = q_b - q_a$ less than (greater than) zero on the lower (upper) one-exciton surface−to a configuration corresponding to "acceptor" excitation−one with q greater than (less than) zero on the lower (upper) surface. Terms with $s \neq s'$ shift the frequency of "precessional" excitation transfer from $2J$ (already accounted for by $G_{s's}(t_d)$) to the slightly higher and lower frequencies corresponding to transitions between *vibronic* levels of the upper and lower one-exciton manifolds. This effect has been neglected in some prior studies of transient absorption from strongly coupled complexes.[10,71]

The various factors $g_{s's}(t_d) = \langle diff_{s'}|diff_s\rangle$ are overlaps between difference-mode states

$$|diff_s\rangle = (\alpha_D\xi_s(\hat{q}) + \beta_D\xi'_s(\hat{q})) \exp\left\{-it_d\left(\frac{\hat{p}^2}{2\mu} + v_s(\hat{q})\right)\right\} \times (\alpha_C\xi_s(\hat{q}) + \beta_C\xi'_s(\hat{q}))|n_0 = 0\rangle \quad \text{(B3)}$$

with $\alpha_I = \boldsymbol{\mu}_a\cdot\boldsymbol{e}_I$ and $\beta_I = \boldsymbol{\mu}_b\cdot\boldsymbol{e}_I$ for $I = C,D$, where $\langle q|n_0 = 0\rangle = (\mu\omega/\pi)^{1/4} \exp\{-(\mu\omega/2)q^2\}$ is the wave function for the lowest difference-mode level of the electronic ground state. The overlaps can therefore be written schematically as

$$g = \underbrace{\alpha\alpha\alpha\alpha}_{C}\underbrace{\xi\xi\xi\xi}_{s'}\underbrace{\xi\xi\xi\xi}_{s} + \beta\alpha\alpha\alpha\xi'\xi\xi\xi + 14 \text{ more terms} \quad \text{(B4)}$$

This representation of g has the same structure as $S(t_d)$ itself prior to averaging over orientations, with ξ and ξ' replacing p and p'. The orientationally averaged overlaps for the cases of parallel and perpendicular polarizations can thus be obtained by transcribing eqs 13 and 14

$$\langle g_{s's}(t_d)\rangle_{||} = \frac{\mu^4}{5}\xi\xi\xi\xi + \frac{\mu^4}{5}\cos\alpha(\xi'\xi\xi\xi + \xi\xi'\xi\xi + \xi\xi\xi'\xi + \xi\xi\xi\xi') + \frac{\mu^4}{15}(1 + 2\cos^2\alpha)(\xi'\xi'\xi\xi + \xi'\xi\xi'\xi + \xi'\xi\xi\xi' + \xi\xi'\xi'\xi + \xi\xi'\xi\xi' + \xi\xi\xi'\xi') + \frac{\mu^4}{5}\cos\alpha(\xi'\xi'\xi'\xi + \xi'\xi'\xi\xi' + \xi'\xi\xi'\xi' + \xi\xi'\xi'\xi') + \frac{\mu^4}{15}\xi'\xi'\xi'\xi' \quad \text{(B5)}$$

$$\langle g_{s's}(t_d)\rangle_{\perp} = \frac{\mu^4}{15}\xi\xi\xi\xi + \frac{\mu^4}{15}\cos\alpha(\xi'\xi\xi\xi + \xi\xi'\xi\xi + \xi\xi\xi'\xi + \xi\xi\xi\xi') + \frac{\mu^4}{30}(3\cos^2\alpha - 1)(\xi'\xi'\xi\xi + \xi'\xi\xi'\xi + \xi'\xi\xi\xi' + \xi\xi'\xi'\xi + \xi\xi'\xi\xi' + \xi\xi\xi'\xi') + \frac{\mu^4}{15}(2 - \cos^2\alpha)(\xi'\xi\xi\xi' + \xi\xi'\xi'\xi) + \frac{\mu^4}{15}\cos\alpha(\xi'\xi'\xi'\xi + \xi'\xi'\xi\xi' + \xi'\xi\xi'\xi' + \xi\xi'\xi'\xi') + \frac{\mu^4}{15}\xi'\xi'\xi'\xi' \quad \text{(B6)}$$

In pursuing analytical expressions for the terms in (B5) and (B6), we write each them as an inner product, $\xi_{s'}{}^{(l)}\xi_{s'}{}^{(k)}\xi_s{}^{(i)}\xi_s{}^{(j)} = \langle kl_{s'}|ij_s\rangle$, between states of the form

$$|ij_s\rangle = \xi_s{}^{(i)}(\hat{q}) \exp\left\{-it_d\left(\frac{\hat{p}^2}{2\mu} + v_s(\hat{q})\right)\right\}\xi_s{}^{(j)}(\hat{q})|n_0 = 0\rangle \quad \text{(B7)}$$

These overlaps must be obtained through second order in λ. We do not rehearse the further details, but simply state the final result

$$\langle kl_{s'}|ij_s\rangle = \langle 0_{s'}|0_s\rangle e^{it_d(\omega_{s'}-\omega_s)/2}\frac{s'^{k+l}s^{i+j}}{4}\left\{1 - \frac{\lambda^2}{\mu\omega} - \frac{(\lambda d)^2}{8} + \frac{\lambda^2}{2\mu\omega}((-1)^{k+l}e^{it_d\omega_{s'}} + (-1)^{i+j}e^{-it_d\omega_s})\right\} + \langle 2_{s'}|0_s\rangle e^{it_d(5\omega_{s'}-\omega_s)/2}s'^{k+l+1}s^{i+j}\frac{\lambda d}{8\sqrt{2}} + \langle 0_{s'}|2_s\rangle e^{it_d(\omega_{s'}-5\omega_s)/2}s'^{k+l}s^{i+j+1}\frac{\lambda d}{8\sqrt{2}} + e^{it_d(\omega_{s'}-\omega_s)/2}s'^{k+l+1}s^{i+j+1}\frac{\lambda^2}{8\mu\omega}((-1)^k + (-1)^l e^{it_d\omega_{s'}})((-1)^i + (-1)^j e^{-it_d\omega_s}) + e^{it_d(5\omega_{s'}-5\omega_s)/2}s'^{k+l+1}s^{i+j+1}\frac{(\lambda d)^2}{32} \quad \text{(B8)}$$

in which $\langle 0_{s'}|0_s\rangle = 1 - (s' - s)^2(\lambda d)^2/16$ and $\langle 2_{s'}|0_s\rangle = -\langle 0_{s'}|2_s\rangle = \lambda d(s' - s)/2^{3/2}$.

Expressions (B2), (B5) or (B6), and (B8) can be substituted in eq 21 to give the emission signal from the strongly coupled complex. The results are compared with numerical simulations in Figure 9.

Acknowledgment. This work was supported by the US NSF and a fellowship (for J.A.C.) from the John Simon Guggenheim Memorial Foundation. We thank Dr. Jörg Zimmerman for helpful discussions and Prof. Susan Dexheimer for encouraging us to further investigate the strong-coupling case. We benefited from Prof. Robert A. Harris's comments on the manuscript. J.A.C. thanks Mark Limont, Marsha Saxton, Young-Kee Kim, and all the members of the Fleming group for their hospitality during his stays in Berkeley; Janine O'Guinn for her help with the manuscript; and Barbara Sklar and Zoë Cina-Sklar for their encouragement, forbearance, and wise counsel throughout.

References and Notes

(1) Bradforth, S. E.; Jimenez, R.; van Mourik, F.; van Grondelle, R.; Fleming, G. R. *J. Phys. Chem.* **1995**, *99*, 16179.
(2) Monshouwer, R.; Baltuška, A.; van Mourik, F.; van Grondelle, R. *J. Phys. Chem. A* **1998**, *102*, 4360.
(3) Chachisvilis, M.; Pullerits, T.; Jones, M. R.; Hunter, C. N.; Sundström, V. *Chem. Phys. Lett.* **1994**, *224*, 345.
(4) Chachisvilis, M.; Fidder, H.; Pullerits, T.; Sundström, V. *J. Raman Spectrosc.* **1995**, *26*, 513.
(5) Jimenez, R.; van Mourik, F.; Yu, J. Y.; Fleming, G. R. *J. Phys. Chem. B* **1997**, *101*, 7350.
(6) Yu, J.-Y.; Nagasawa, Y.; van Grondelle, R.; Fleming, G. R. *Chem. Phys. Lett.* **1997**, *280* 404.
(7) Vos, M. H.; Jones, M. R.; Hunter, C. N.; Breton, J.; Lambry, J.-C.; Martin, J. L. *Biochemistry* **1994**, *33*, 6750.
(8) Stanley, R. J.; Boxer, S. G. *J. Phys. Chem.* **1995**, *99*, 859.
(9) Roszak, A. W.; Howard, T. D.; Southhall, J.; Gardiner, A. T.; Law, C. J.; Isaacs, N. W.; Cogdell, R. J. *Science* **2003**, *302*, 1969.
(10) Novoderezhkin, V.; Monshouwer, R.; van Grondelle, R. *J. Phys. Chem. B* **2000**, *104*, 12056. See also: Novoderezhkin, V.; van Grondelle, R. *J. Phys. Chem. B* **2002**, *106*, 6025.
(11) Förster, Th. in *Modern Quantum Chemistry*, part III.; Sinanoglu, O.; Ed; Academic Press: New York, 1965; pp 93−137.
(12) Rackovsky, S.; Silbey, R. *Mol. Phys.* **1973**, *25*, 61.
(13) Soules, T. F.; Duke, C. B. *Phys. Rev. B* **1971**, *3*, 262.
(14) Compare our results with Figures 3 and 4 of ref 1 and Figures 5 and 6 of ref 2.

(15) For a similar electronic oscillation in the pump−probe anisotropy of the B820 dimeric subunit of LH1, see Figure 3b of Kumble, R.; Palese, S.; Visschers, R. W.; Dutton, P. L.; Hochstrasser, R. M. *Chem. Phys. Lett.* **1996**, *261*, 396. These data also show vibrational-period oscillations (∼170 cm^{-1}) in the isotropic stimulated emission signal; see the lowest panel of Figure 2b.

(16) See also Figures 5 and 6 of Zhu, F.; Galli, C.; Hochstrasser, R. M. *J. Chem. Phys.* **1993**, *98*, 1042.

(17) In the equal-energy case the two site energies are the same on average, so the donor and acceptor designations are arbitrary. We refer to donor-excited and acceptor-excited states to identify an initially excited state and one excited via energy transfer, but all our calculations treat both chromophores on the same footing.

(18) Continuous-wave spectra of this dimer model have been well documented: Fulton, R. L.; Gouterman, M. *J. Chem. Phys.* **1964**, *41*, 2280.

(19) John Jean investigated the pulse-driven dynamics of a similar system in contact with a thermal bath: Jean, J. M. *J. Phys. Chem. A* **1998**, *102*, 7549.

(20) Matro, A.; Cina, J. A. *J. Phys. Chem.* **1995**, *99*, 2568, and references therein.

(21) For a description of model Hamiltonians for photosynthetic pigment−protein complexes and the interpretation of their optical spectra in a density-matrix treatment, see: Renger, T.; May, V.; Kühn, O. *Phys. Rep.* **2001**, *343*, 137.

(22) Although the last of these parameters is irrelevant in a pump−probe experiment, it will play a role in nonlinear wave packet interferometry studies of electronic energy transfer[23] and state reconstruction.[24]

(23) Cina, J. A.; Kilin, D.; Humble, T. S. *J. Chem. Phys.* **2003**, *118*, 46.

(24) Humble, T. S.; Cina, J. A. *Phys. Rev. Lett.* **2004**, *93*, 060402.

(25) The sign in eq 11 is chosen so that increased stimulated emission leads to a positive change in *S*.

(26) We neglect the effects of pulse overlap, which should be insignificant for the short pulses of differing center frequency that we employ.

(27) Ungar, L. W.; Cina, J. A. *Adv. Chem. Phys.* **1997**, *100*, 171, Appendix A. The equivalence between stimulated and spontaneous emission is approximate, as it neglects the frequency dependence of the density of states of the radiation field in the latter process.

(28) Gelin, M. F.; Pisliakov, A. V.; Domcke, W. *Phys. Rev. A* **2002**, *65*, 062507.

(29) Orientational factors similar to those in eqs 13 and 14 appear in expressions for the infrared nonlinear-optical response of coupled anharmonic vibrations: Golonzka, O.; Khalil, M.; Demirdöven, N.; Tokmakoff, A. *J. Chem. Phys.* **2001**, *115*, 10814.

(30) For an arbitrary choice of pump- and probe−pulse polarizations, the orientationally averaged signal can be written

$$S(t_d) = \sum_{\chi,\chi',\delta,\delta'} s_{\chi\chi'\delta\delta'} e_{C\chi} e_{C\chi'} e_{D\delta} e_{D\delta'}$$

where the sum is over lab-frame components of the pump (χ,χ') and probe (δ, δ'). Because the sample has mirror symmetry, we have for instance, $s_{ZZZY} = s_{ZZZ(-Y)}$. But changing the *sign* of the angle between pump and probe polarizations can have no effect, so $s_{ZZZ(-Y)} = -s_{ZZZY}$, and it follows that $s_{ZZZY} = 0$. Application of this argument to other "odd index" components leads to the result that the pump−probe signal in its entirety (not just the stimulated emission term) can be expressed as a linear combination of parallel and perpendicular "base signals": $S = S_{\|} \cos^2\Gamma + S_{\perp} \sin^2\Gamma$, where Γ is the angle between the polarizations of the two pulses. The absence of a $\cos\Gamma\sin\Gamma$ cross-term can be checked for the stimulated emission component by explicitly averaging eq 11.

(31) Each term in eqs 13 and 14 can be identified with a Liouville-space pathway and the corresponding nonlinear optical response function, as is described in Mukamel, S., *Principles of Nonlinear Optical Spectroscopy*; Oxford University Press: New York, 1995.

(32) The basis was truncated at 110 states, 55 in each electronic state with $n_a + n_b \leq 9$.

(33) Cohen-Tannoudji, C.; Diu, B.; Laloë, F. *Quantum Mechanics* Vol. I.; John Wiley & Sons: New York, 1977; complement G_V.

(34) For instance,

$$\langle (n'_a, n'_b)_0 | \langle 0|c|e\rangle | (n_a, n_b)_e \rangle = \frac{i}{2} A_C \sigma_C \sqrt{2\pi} \langle (n'_a, n'_b)_0 | (n_a, n_b)_e \rangle \times \exp\left\{ i\Phi_C - \frac{\sigma_C^2}{2} [\omega(n'_a + n'_b - n_a - n_b) + \Omega_C - \epsilon_e]^2 \right\}$$

where $e = 1$ or $1'$.

(35) The surface-crossing description of energy and vibrational-coherence transfer given here can be re-framed in terms more closely aligned with the spectral-overlap picture of Förster theory, and conversely. A coherently vibrating donor molecule exhibits an oscillatory time-dependent emission spectrum. At the inner turning point of such a short-pulse-excited vibration, the peak emission frequency matches the peak absorption of an equal-site-energy acceptor molecule in its electronic ground state, facilitating the reabsorption of donor-emitted light by the acceptor and launching a Franck−Condon-excited wave packet in the acceptor whose phase of motion matches that of the donor. Similar time-dependent spectral descriptions can be given for various differences in site energy between donor and acceptor, and the relative phases of vibrational motion in the two molecules predicted accordingly. See the comments below on ref 52, which generalizes Förster theory along lines similar to these.

(36) The initial anisotropy value 0.4 was first observed in picosecond experiments on fluorescein dyes: Fleming, G. R.; Robinson, G. W. *Chem. Phys.* **1976**, *17*, 91.

(37) Qian, W.; Jonas, D. M. *J. Chem. Phys.* ***2003***, *119*, 1611.

(38) Reference 37 develops an analogy in electronic structure between energy-transfer dimers and square-shaped molecules with doubly degenerate excited electronic states. In light of this analogy, it is interesting to note the appearance of roughly in-phase quantum beats between parallel and perpendicular pump−probe measurements on the degenerate Q_x and Q_y bands of cadmium tetraphenylporphyrin (assigned to vibrational coherence in stimulated emission and excited-state absorption); see Figure 2 of Galli, C.; Wynne, K.; LeCours, S. M.; Therien, M. J.; Hochstrasser, R. M. *Chem. Phys. Lett.* **1993**, *206* 493.

(39) A run to $t_d = 100\tau_{vib}$ on a reduced sample of 110 realizations under the same conditions as Figure 3 exhibits undamped vibration-period oscillations in both components of the polarized emission and a long-time anisotropy in the same range.

(40) Pump−probe calculations have been reported for dimers with separate intramolecular vibrations and unequal site energies. These were compared with experiments from the LHC−II antenna of green plants, the B820 subunit of LH1, and the pigment−protein complexes of cyanobacteria. See ref 20 and Section 9.2 of ref 21.

(41) Jean, J. M. *J. Chem. Phys.* **1994**, *101*, 10464.

(42) Rapid excitation transfer from site to site leads to exchange narrowing of the absorption spectrum, a process that has been analyzed in terms of dichotomic Markovian site-energy noise in circular aggregates: Bakalis, L. D.; Mircea, C.; Knoester, J. *J. Chem. Phys.* **1999**, *110*, 2208. In the present instance, exchange narrowing of the dimer absorption spectrum is a consequence of relocating the potential energy minima to $(q_a, q_b) = (d/2, d/2)$ (see Figure 8); the distance from the Franck−Condon point is decreased to $d/\sqrt{2}$ and the absorption bandwidth to the adiabatic levels thereby narrowed by $1/\sqrt{2}$ relative to the site-state absorption of the weak-coupling case.

(43) Yang, M.; Fleming, G. R. *Chem. Phys.* **2002**, *282*, 163.

(44) Zhang, W. M.; Meier, T.; Chernyak, V.; Mukamel, S. *J. Chem. Phys.* **1998**, *108*, 7763.

(45) The theories of refs 43 and 44 are based on separating vibrations that do or do not couple *crude* (i.e., nuclear coordinate independent) electronic eigenstates, rather than the nuclear-coordinate-dependent adiabatic electronic states used here. While the roles of these groups of coordinates resemble those of our *q* and *Q*, respectively, the identification is therefore not exact.

(46) $\sigma_C = 0.0001\tau_{vib}$ in the numerical calculation.

(47) Jean, J. M.; Fleming, G. R. *J. Chem. Phys.* **1995**, *103*, 2092.

(48) Bihary, Z.; Zadoyan, R.; Karavitis, M.; Apkarian, V. A. *J. Chem. Phys.* **2004**, *120*, 7576; see Figure 6.

(49) Davis, A. V.; Wester, R.; Bragg, A. E.; Neumark, D. M. *J. Chem. Phys.* **2003**, *119*, 2020.

(50) Ashkenazi, G.; Banin, U.; Bartana, A.; Kosloff, R.; Ruhman, S. *Adv. Chem. Phys.* **1997**, *100*, 229; see especially Figure 4.

(51) Wang, Q.; Schoenlein, R. W.; Peteanu, L. A.; Mathies, R. A.; Shank, C. V. *Science* **1994**, *266*, 422.

(52) Jang, S.; Jung, Y.; Silbey, R. J. *Chem. Phys.* **2002**, *275*, 319.

(53) Recall that the remaining terms in eqs 13 and 14, which account for electronic interference, are found to be small when E_{FC} is larger than 2*J*.

(54) Electronic interference persists, however, for the system with weaker vibration-excitation coupling shown in Figure 7. In this case there are three rather than two independent contributions to $S_{\|}$ and $S_{\perp}$, plotted in Figure 11, and the individual terms cannot be separated.

(55) Jang and Silbey analyzed the line shapes of multichromophoric macromolecules with reference to single-molecule measurements on light-harvesting complexes: Jang, S.; Silbey, R. J. *J. Chem. Phys.* **2003**, *118*, 9312 and 9324.

(56) Theoretical studies relevant to LH2 examined the effects of inter-chromophore coupling, ring size, and vibrational spectral density on exciton delocalization and energy-transfer: Subramanian, V.; Evans, D. G. *J. Phys. Chem. B* **2004**, *108*, 1085.

(57) Vibrational quantum beats were not observed, however, in femtosecond pump−probe polarization experiments on the B850 band of the peripheral light-harvesting complex LH2, despite its structural similarity to LH1: Nagarajan, V.; Johnson, E. T.; Williams, J. C.; Parson, W. W. *J. Phys. Chem. B* **1999**, *103*, 2297.

(58) Pollard, W. T.; Friesner, R. A. *J. Chem. Phys.* **1994**, *100*, 5054.

(59) Cina, J. A.; Harris, R. A. *Ultrafast Phenomena* IX; Knox, W., Barbara, P., Eds.; Springer-Verlag: Berlin, 1994; pp 486−487.

(60) Silbey, R.; Harris, R. A. *J. Phys. Chem.* **1989**, *93*, 7062.

(61) Ungar, L. W.; Cina, J. A. *J. Phys. Chem. A* **1998**, *102*, 7382.
(62) Kelley, A. M. *J. Chem. Phys.* **2003**, *119*, 3320.
(63) Ishikawa, N. *J. Porphyr. Phthalocya.* **2001**, *5*, 87.
(64) Prall, B. S.; Parkinson, D. Y.; Fleming, G. R.; Yang, M.; Ishikawa, N. *J. Chem. Phys.* **2004**, *120*, 2537.
(65) With an arbitrary difference in site energies, the crossing point for a q_a-wave packet in the donor state is given by $q_{ax} = d(\epsilon_1 - \epsilon_{1'})/(2E_{FC})$. The donor emission line is given by $q_{ar} = d(\epsilon_1 + E_{FC} - \Omega_D)/(2E_{FC})$ and that for acceptor emission by $q_{br} = d(\epsilon_{1'} + E_{FC} - \Omega_D)/(2E_{FC})$. Since $q_{br} = q_{ar} - q_{ax}$, and $q_{ar} = 2d$ in our calculations, we have $q_{br} = 2d - q_{ax}$. The newly launched wave packet in the acceptor state must travel the same distance in q_b to its first pass through the resonance window as the continuing q_a-wave packet in the donor state does to reach its resonance window at the outer turning point. This coincidence guarantees that bursts of donor and acceptor emission will occur simultaneously, regardless of the site energy difference. When that difference is nonzero, however, a second sequence of acceptor emission bursts occurs during each transferred wave packet's second, fourth, etc. passage through q_{br}.
(66) Jean and Fleming noted a related broadening of the vibrational power spectrum in their calculations on a strongly coupled one-dimensional curve-crossing system. See Figures 6 and 8 of ref 47.
(67) See the residual power spectra in Figure 8 of ref 2 and also Figures 5 and 6 of ref 4.
(68) For an investigation of the role of vibrational fluctuations on photosynthetic *electron* transfer, see: Balabin, I. A.; Onuchic, J. *Science* **2000**, *290*, 114.
(69) Herek, J. L.; Wohlleben, W.; Cogdell, R. J.; Zeidler, D.; Motzkus, M. *Nature* **2002**, *417*, 533.
(70) Because the probe is here assumed to be shorter than both electronic and vibrational time-scales, we replace the resonance curves in Figure 8 with their anti-diagonal tangent lines.
(71) Chachisvilis, M.; Sundström, V. *Chem. Phys. Lett.* **1996**, *261*, 165.